Experimental characterization of the mechanical behaviour and the failure of multi-sheet and multi-material spot welded assembly

Rami Tounsi, Grégory Haugou, Fahmi Chaari, Nicolas Leconte, Eric Markiewicz

Experimental characterization of the mechanical behaviour and the failure of multi-sheet and multi-material spot welded assembly

R. Tounsi[a], G. Haugou[a], F. Chaari[a], N. Leconte[a], E. Markiewicz[a,*]

[a] *Univ. Polytechnique Hauts-de-France, CNRS, UMR 8201 - LAMIH, F-59313 Valenciennes, France*

Abstract

An experimental investigation of the mechanical behaviour of three-sheet multi-material spot welded assembly is performed. An experimental device based on the Arcan principle is developed to test the three-sheet spot welded specimen under pure opening mode, pure shear mode and mixed opening/shear mode with three nugget sizes. A significant effect of the loading angle is reported and explained by three identified failure modes as a pull-out failure mode (pure opening), an inter-facial failure mode (pure shear) and a mixed pull-out/inter-facial failure mode (mixed opening/shear). A pronounced effect of nugget diameter size is reported on the ultimate force and the dissipated energy. A preliminary study of the strain-rate sensitivity of the three-sheet multi-material spot welded assembly is also undertaken.

Keywords:

Spot welds, Multi-sheet, Multi-material, Experiments, Dynamic testing

1. Introduction

Reducing the weight in the automotive industry improves fuel efficiency and reduces greenhouse gas emissions, but the mechanical strength required

---

*Corresponding author

Email addresses: `tounsi.f@gmail.com` (R. Tounsi), `gregory.haugou@uphf.fr` (G. Haugou), `fahmi.chaari@uphf.fr` (F. Chaari), `nicolas.leconte@uphf.fr` (N. Leconte), `eric.markiewicz@uphf.fr` (E. Markiewicz)

to meet crash safety requirements has to be maintained. The weight reduction is achieved through the increasing development and use of lightweight materials or by reducing the sheet thicknesses made of Ultra High Strength Steels (UHSS). Up to now, Resistance Spot Welding (RSW) remains the most commonly used (and the cheaper) process to join two or more sheets (around four thousands spot welds are performed to assemble the body in white).

Using this RSW process, it is possible and easy to joint different steel grades combinations and sheet thicknesses. Joining multi-sheet (more than two) by RSW is considered in this study. Compared to two-sheet spot welded assemblies, joining multi-sheet is significantly more complicated. Indeed, the use of different steel grades combinations and different sheet thicknesses in the multi-layer spot welded assemblies complicates not only the welding process but also the investigation of their mechanical behaviour up to failure that represents a new challenge. Despite the increasing use of this new generation of RSW, their mechanical behaviour is not yet well studied. To the knowledge of the authors, most of the published works consider two-sheet spot welded assemblies.

Since 1958, mechanical tests have been discussed [1, 2, 3] in particular for pure tension, tension-shear and peel specimens. For these types of tests, a large part of the sheet sample deforms plastically, in particular far from the spot weld. Thus, it contributes significantly to the global behaviour. Moreover, it is difficult to express the failure properties because the tensile/shear load ratio conditions vary during the test. More recently, many researchers [4, 5, 6, 7, 8, 9] have proposed to adapt the Arcan tests to investigate the failure characteristics of two-sheet spot welded assemblies under combined loading conditions. Indeed, Arcan tests have advantages over standard tests that the plates contribution around the weld nugget in the mechanical response is reduced. Moreover, it allows tensile (mode I) and shear (mode II) loads to be pure or combined and well controlled. However, these devices are characterized by a large mass that generates inertial forces during the dynamic loading. Thus, they can be used only under quasi-static loading conditions. To overcome this limitation and to investigate the strain rate sensitivity of spot welds in dynamic conditions,

2

Langrand and Markiewicz [8] have proposed an experimental device with a reduced mass to cope with these inertial forces.

The published experimental studies previously presented are limited to two-sheet spot welded assemblies. However, the mechanical behaviour of the multi-sheet, multi-steel grades spot-welded assemblies is not yet well studied. Few works relate the study of the mechanical strength under quasi-static loading using conventional tensile-shear specimens. In fact, Pouranvari et al. [10, 11] and Tavasolizadeh et al. [12] have been interested in the nugget growth, mechanical performance and failure behavior of three-sheet low carbon steel resistance spot welds. Nielsen et al. [13] have investigated the weldability of a thin, low-carbon steel sheet to high-strength low-alloy (HSLA) and AHSS. Recently, Wei et al. [14] have studied the weldability and mechanical properties of similar and dissimilar resistance spot welds of three-layer advanced high strength steels. All these works have used the tensile-shear tests to study the mechanical behaviour of three-sheet spot welded assemblies. This type of experimental specimen is characterized by an important contribution of the plates in the global response. In this context, an advanced experimental procedure based on Arcan test is proposed in this work to characterize the mechanical behaviour of a three-sheet spot welded assembly made of a thin low-carbon steel sheet and two thicker UHSS sheets. The proposed device allows the investigation of the spot welded assembly under pure and combined modes I/II loading conditions. Thus, the loading modes I/II are combined and well controlled, with a reduced contribution of the plates strength surrounding the weld nugget in the macroscopic response. The mechanical behaviour, the failure modes and the strain-rate sensitivity of this multi-sheet and multi-steel grades spot-welded assembly are investigated.

The first section presents the studied three-sheet spot welded assembly and the proposed experimental device. The experimental results are presented in the second section. In the third section, the influences of the loading angle and the nugget size on the mechanical behaviour of the three-sheet spot welded assembly are discussed. Based on the experimental results, the parameters of

3

⁶⁶ a macroscopic force-based failure criterion dedicated to FE crash modelling are
⁶⁷ identified. Finally, as a first attempt, the strain rate sensitivity of the spot
⁶⁸ welded assembly is discussed in the fourth section.

2. Experimental characterization of the mechanical behaviour of three-sheet multi-steel grades spot welded assembly

2.1. Studied spot weld specimens

⁷² The studied spot welded assembly consists of three sheets and involves two
⁷³ steel grades: (P1) is 2 mm thick and made of 22MnB5 ultra-high strength steel,
⁷⁴ (P2) is 0.65 mm thick and made of DX54D mild steel and (P3) is 1.6 mm thick
⁷⁵ and made of 22MnB5 (figure 1). The DX54D mild steel grade is classified as an
⁷⁶ alloy quality low carbon steel. The 22MnB5 is classified as ultra-high strength
⁷⁷ steel. It is considered as an efficient way to combine the superior mechanical
⁷⁸ properties, weight/cost reduction and crash safety. This kind of steel grade is
⁷⁹ intended for structural parts and safety in the automotive sector. Two metallic
⁸⁰ rigs have been designed and joined each free face of the spot welded assembly
⁸¹ (figure 1). The role of the two rigs is to ensure the connection between the spot
⁸² welded specimen and the device. These rigs are made of Z160 steel alloy, and
⁸³ are 6 mm thick. They are rigidly linked to the free faces of the sample by a
⁸⁴ process wich is not detailed in this paper due to a confidentiality agreement
⁸⁵ with our industrial partner. The mechanical strength of this connection has
⁸⁶ been experimentally checked to be higher than the spot weld one. In addition,
⁸⁷ this connection ensures an isotropic loading of the spotweld. [8]
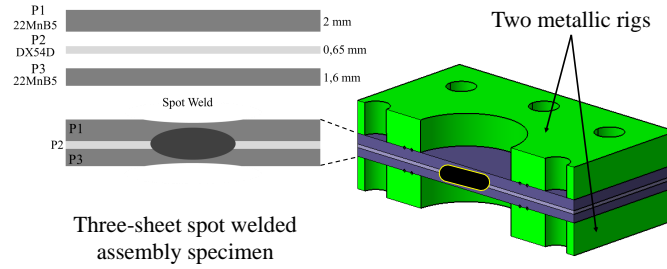
4

Figure 1: Studied spot welded specimen

⁸⁸ The spot welding process was performed by our industrial partner according
⁸⁹ to his know-how. Depending on the welding conditions, different weld nugget
⁹⁰ sizes are possible according to internal quality rules. According to internal rules
⁹¹ criteria, the spot welds are classified in two ranges: Acceptable Nugget and
⁹² Not Acceptable Nugget. Figure 2 shows the classification of the spot weld in
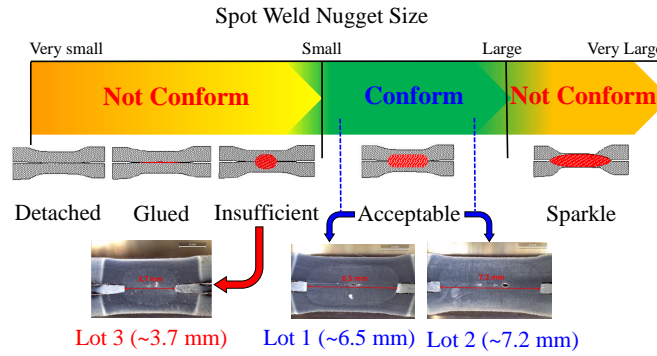⁹³ accordance with Nugget size.

Figure 2: Spot welds quality according to the nugget size and the three considered Lots

⁹⁴ In this study, three lots (figure 2) are considered as follows :

⁹⁵ • Lot 1 : Acceptable Nugget (Nugget Conform A small size);

₉₆ • Lot 2 : Acceptable Nugget (Nugget Conform B large size);

₉₇ • Lot 3 : Not Acceptable Nugget (Nugget Not Conform C).

₉₈ According to the different loading conditions, three types of specimens
₉₉ are proposed to perform three loading configurations. The first configuration
₁₀₀ called "Configuration 1-3" corresponds to spot weld specimen "S.1-3" composed
₁₀₁ by three square plates (60 mm x 60 mm). The second configuration called
₁₀₂ "Configuration 1-2" corresponds to spot weld specimen "S.1-2" composed by
₁₀₃ two square plates (P1 and P2 : 60 mm x 60 mm) and a circle plate (P3 : 25
₁₀₄ mm). The third configuration is the inverse of the second configuration called
₁₀₅ "Configuration 2-3" corresponds to spot weld specimen "S.2-3" composed by a
₁₀₆ circle plate (P1 : 25 mm) and two square plates (P2 and P3 : 60 mm x 60 mm).
₁₀₇ Figure 3 presents a schematization of the specimen different configurations.
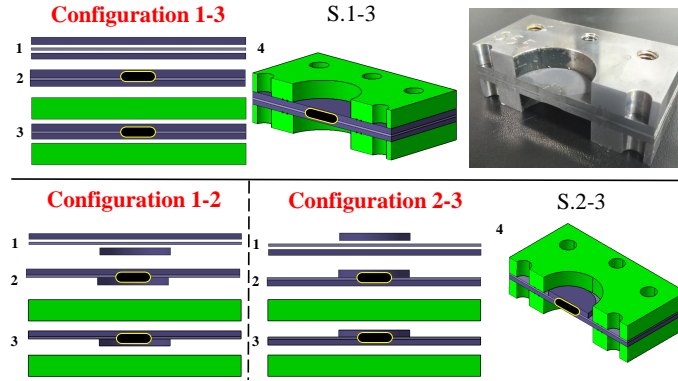

Figure 3: Loading configurations 1-3, 1-2 and 2-3

₁₀₈ *2.2. Experimental device*

₁₀₉ An experimental device based on the Arcan principle is developed to
₁₁₀ investigate the three-sheet spot welded specimen behaviour and failure modes
₁₁₁ in pure and combined loading conditions. The proposed device is composed by
₁₁₂ rigid counterparts that have been designed for each angular position as presented
₁₁₃ in figure 4. By convention, the pure tension (opening mode) is obtained for $\psi =$
₁₁₄ 0 °, and on the other end of range, the pure shear for $\psi = 90$ °. The specimen is

₆

¹¹⁵ positioned on the device by two centring pins and fixed with six screws (figure
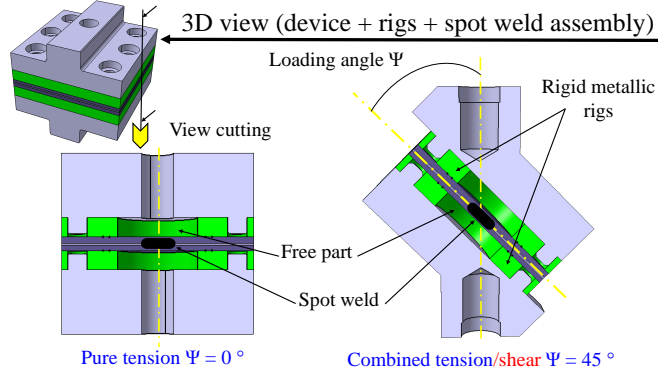
¹¹⁶ 4).

Figure 4: The proposed device with the studied specimen "three-sheet spot welded assembly + two rigid metallic rigs"

¹¹⁷   The geometry of the experimental device has been designed thanks to FE

¹¹⁸ simulations using approximate material data. On the one hand, the linear

¹¹⁹ dynamics response is simulated to ensure that natural frequencies will be avoided

¹²⁰ for the considered loading velocities. On the other hand, all mechanical design

¹²¹ for the number and the location of the screws, the thickness of the counterparts,

¹²² is accomplished thanks to numerical simulations. The choice of the load cell is

¹²³ also based on the obtained results. The final design realises a compromise

¹²⁴ between mechanical strength and reduced inertia effects (Figure 5).
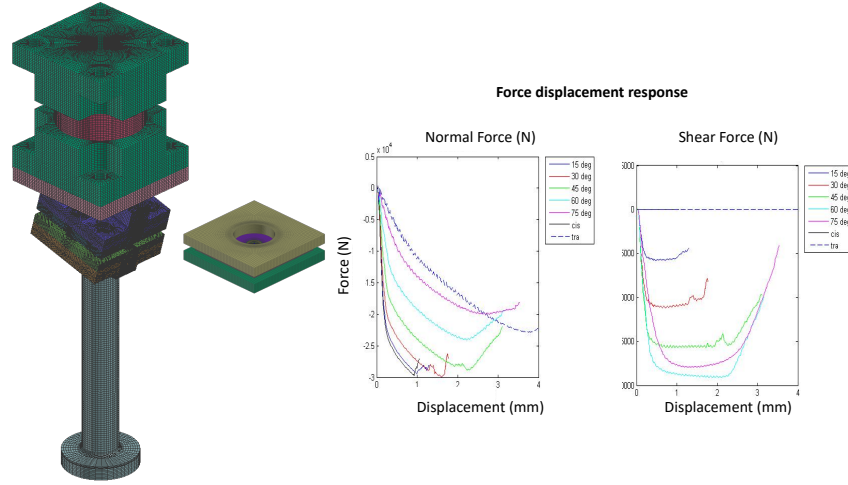
Figure 5: Overview of FE simulations carried out

The tests are carried out on a high speed hydraulic machine (INSTRON VHS 65/20). In a first step, only quasi-static loading conditions are applied on the specimens. The hydraulic actuator moves along the vertical axis (z) with a loading speed of $V = 0.001m/s$. The forces along the three main directions of the machine (Fx; Fy and Fz) are recorded during experiments by using a tri-axial load cell (Kistler 9367C). The load cell links the upper part of the device to the hydraulic machine with four screws. The rotations are not permitted. The bottom part of the device is connected to the hydraulic actuator by a stiff rod. The actuator is initially not in contact with the stiff rod. This contact is only established when the actuator reaches its target velocity. In quasi static loading, the velocity remains constant during all the test, until the failure of the specimen. Figure 6 shows raw data for typical force and displacement measurements. However, for higher loading velocities, it becomes more difficult to keep the closed loop regulation of the actuator due to the relative brittle behaviour of the considered spot weld.
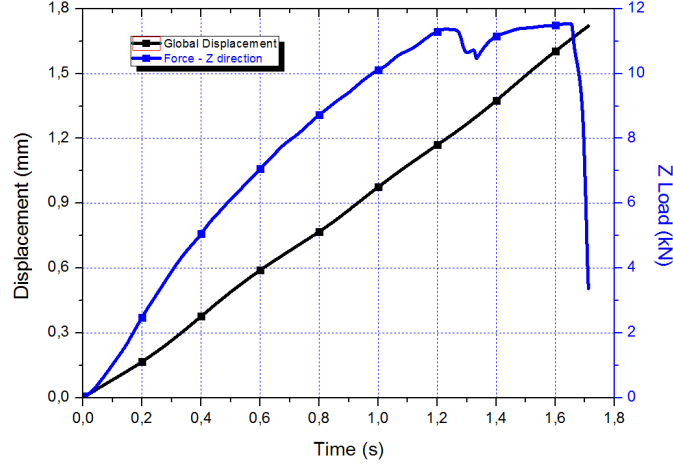
8

Figure 6: Typical raw data on high speed hydraulic machine

The displacement is measured by a LVDT sensor **in the vertical direction**, with a measurement range equal to 300 mm and an error of 0.15 mm. Figure 7 shows the complete set up used for the experiments.
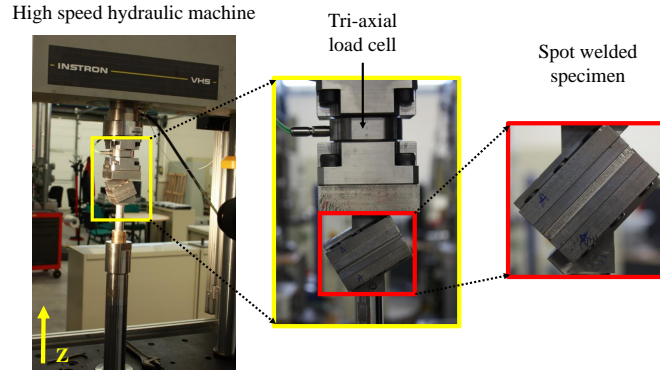

Figure 7: Experimental set-up for testing spot-welded specimens

A special set-up is designed for centring the spot weld assembly with the free zone center to ensure that the principal axe of the spot weld is collinear with the loading direction. The small tolerances imposed to manufacture the specimen

9

¹⁴⁶ allow to neglect the bending moments. It has been verified that in plane X and

¹⁴⁷ Y force components are not significant compared to vertical Z force component.

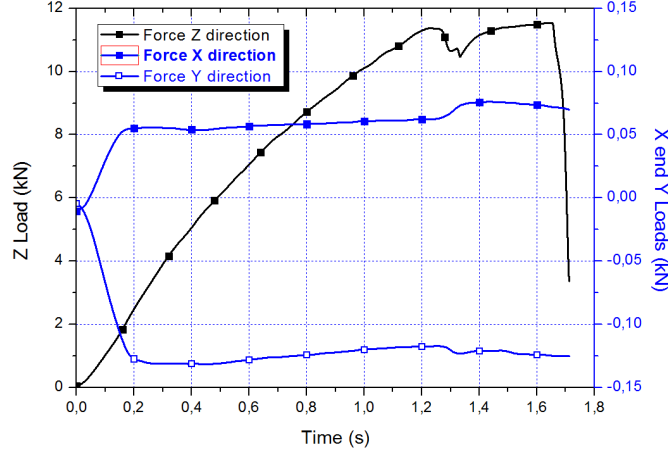¹⁴⁸ This is illustrated in Figure 8 where the three force components are measured.

Figure 8: Typical XYZ force components measured with the tri-axial load cell obtained for ψ = 45 °

¹⁴⁹ Thus, only a resultant force F is considered at the center of the specimen.

¹⁵⁰ The normal (N) and shear (T) force components can be expressed with respect

¹⁵¹ to the loading angle ψ (Eqs. 1 and 2).

$$N(t) = F(t) * cos(\psi) \tag{1}$$

¹⁵² and

$$T(t) = F(t) * sin(\psi) \tag{2}$$

¹⁵³ **3. Experimental results**

¹⁵⁴ To study the mechanical behaviour and the failure of the three-sheet multi-

¹⁵⁵ steel grades spot welded assembly, three possible configurations (1-2), (2-3) and

¹⁵⁶ (1-3) have been tested.

10

3.1. Configurations (1-2) and (2-3)

158   Preliminary experimental results suggest that the mechanical behaviour of
159 the studied three-sheet spot weld assemblies (S.1-2 and S.2-3) are similar for the
160 configurations "1-2" and "2-3". In fact, for both configurations the experimental
161 response corresponds mainly to the behaviour of the middle plate made of
162 DX54D mild steel, because the thick plates made of 22MnB5 UHSS are much
163 more rigid compared to the plate made of DX54D. This remark holds true for
164 the pure tensile, pure shear and mixed mode $\psi = 45$ °. Thus, in the following
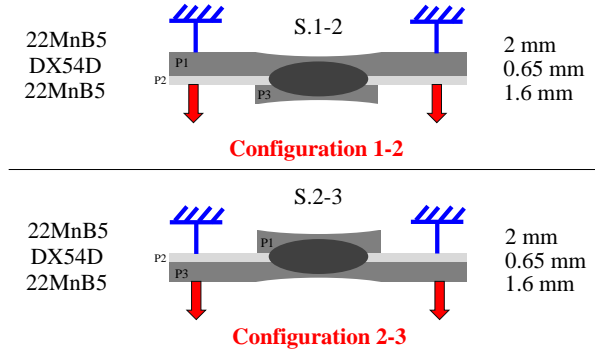165 only the experimental results of configuration "1-2" are considered.

Figure 9: "1-2" and "2-3" configurations

166   The analysis of the failure mode for $\psi < 90$ ° in configuration 1-2 shows that
167 the spot weld is not loaded (figure 10) and that the failure of the assembly is
168 caused by the punching of the middle plate (DX54D) by the circle top plate P_3
169 made of 22MnB5. Therefore, only the shear pure mode ($\psi = 90$ °) is considered
170 for the configuration "1-2". Figure 11 shows the failure mode of the considered
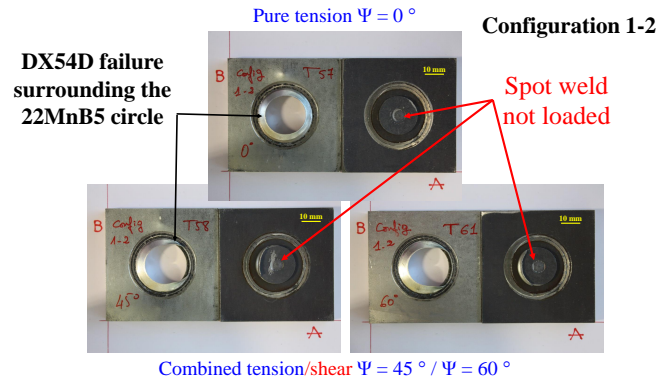171 test.

Figure 10: Failure modes for the pure opening test ($\psi = 0$ °) and for mixed I/II modes ($\psi = 45$ ° and $\psi = 60$ °) in configuration "1-2"

As shown in figure 12, for $\psi = 90$ ° in the configuration 1-2, the force increases progressively with the displacement until a maximum value of force is reached. Then, a progressive decrease of the load is observed up to complete failure.
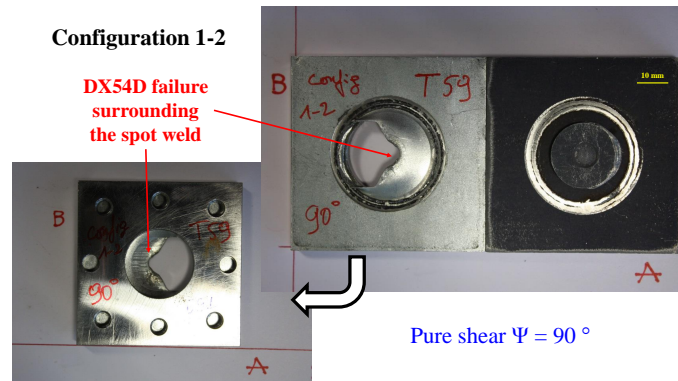

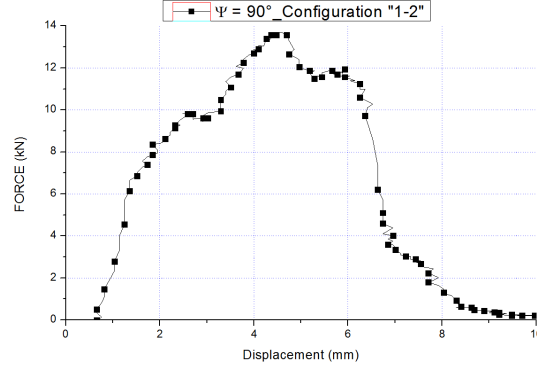Figure 11: Failure mode for the pure shear test in configuration "1-2" ($\psi = 90$ °)

Figure 12: Force vs. displacement for the pure shear test in configuration "1-2" ($\psi = 90$ °)

3.2. Configuration (1-3)

Considering the configuration "1-3", five loading angles have been considered in this investigation: $\psi = 0$ ° for the pure opening mode, $\psi = 30$ °, $\psi = 45$ °, $\psi = 60$ ° for the mixed I/II modes and $\psi = 90$ ° for the pure shear mode. A set of three tests has been performed for each loading configuration. A good reproducibility is checked and the dispersions are not significant. So, the mean value of the three responses is calculated.

3.2.1. Force-displacement responses

Figure 13 shows a typical force vs. displacement response of three-sheet spot welded assembly. The response may be divided into three phases, which can be described as follows:

- Phase 1 : characterised by an elastic-plastic response of the spot weld;

- Phase 2 : an ultimate force is reached;

- Phase 3 : sudden or progressive failure of the assembly depending on the loading angle.

13
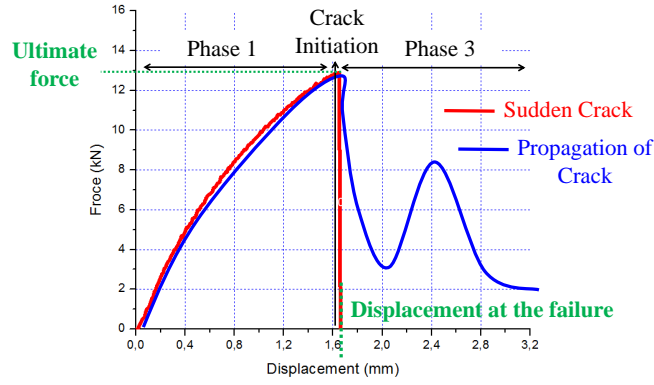
Figure 13: Typical force vs. displacement response of three-sheet spot weld assembly

The force vs. displacement are reported for all Lots (Lot 1, Lot 2 and Lot 3). The experimental responses have similar shape. For this reason, only responses for Lot 1 are presented in this section. A discussion on the nugget quality and diameter size effects is realised in the section (4.2). Figure 14 presents force vs. displacement responses for each loading angle ψ : pure opening mode, pure shear mode and mixed opening/shear mode (Lot 1 / configuration "1-3").

(a) $\psi = 0°$ pure opening mode

(b) $\psi = 90°$ pure shear mode

(c) $\psi = 30°$ mixed opening/shear mode

(d) $\psi = 45°$ mixed opening/shear mode

(e) $\psi = 60°$ mixed opening/shear mode
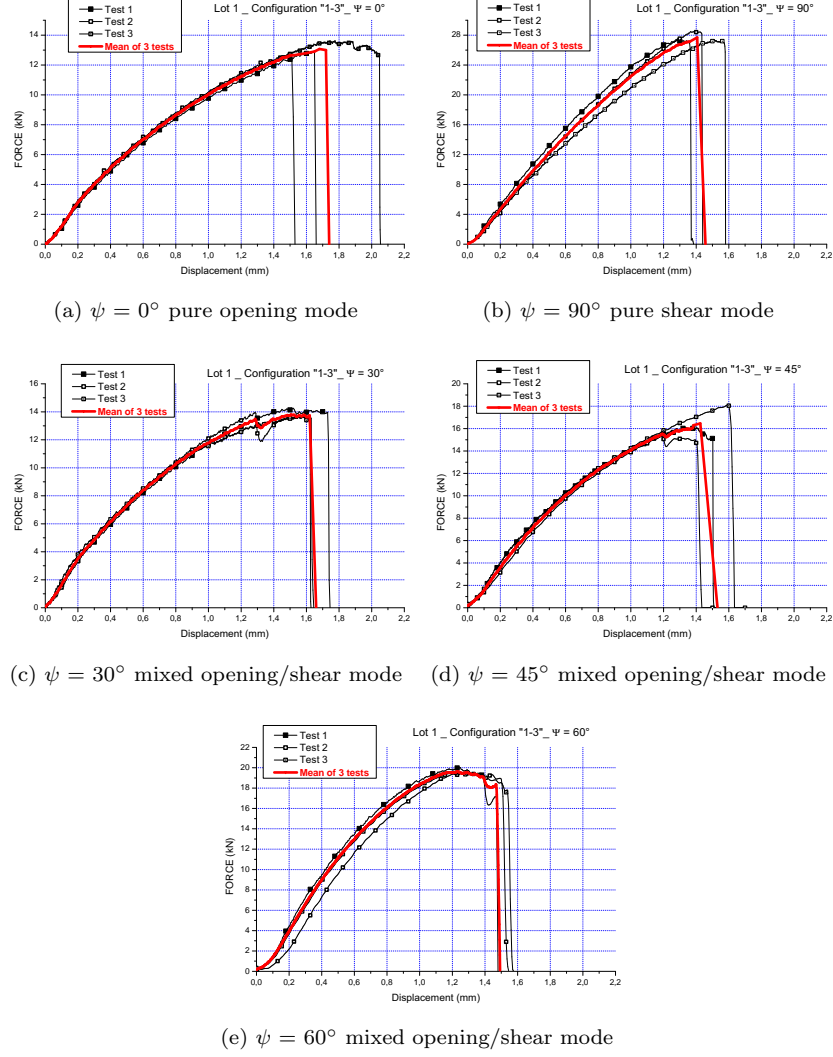
Figure 14: Force vs. displacement responses for pure opening mode (a) $\psi = 0°$, pure shear mode (b) $\psi = 90°$ and mixed opening/shear mode (c) $\psi = 30°$, (d) $\psi = 45°$, (e) $\psi = 60°$

¹⁹⁷ Based on the experimental responses presented in figure 14, the mean
¹⁹⁸ ultimate force and the relative average dispersion are calculated as follows :

$$\bar{F}_{Ultimate} = \frac{1}{n} \sum_{i}^{n} F_{Ultimate}(i), n = 3 \tag{3}$$

15

¹⁹⁹ and

$$Coefficient\ of\ mean\ deviation: \bar{D}(\%) = \frac{1}{n}\sum_{i}^{n}\left|\frac{F_{Ulimate}(i) - \bar{F}_{Ulimate}}{\bar{F}_{Ulimate}}\right| \times 100, n = 3 \tag{4}$$

²⁰⁰   Table 1 presents the mean ultimate force for different loading angle.

Table 1: Ultimate forces for different loading angles

	Pure opening $\psi = 0°$	Mixed opening/shear			Pure shear $\psi = 90°$
		$\psi = 30°$	$\psi = 45°$	$\psi = 60°$	
Test 1 (kN)	12.87	14.25	16.18	21.45	27.29
Test 2 (kN)	12.79	13.96	15.12	19.35	28.46
Test 3 (kN)	13.62	13.70	18.08	19.46	27.38
$\bar{F}_{Ulimate}$ (kN)	13.09	13.97	16.46	20.08	27.71
$\bar{D}$ (%)	2.68	1.33	6.56	4.52	1.8

²⁰¹   The mean displacement at failure and the dissipated energy coupled with the
²⁰² relative average dispersion are also calculated using the equations Eqs.3 and 4
²⁰³ applied to the displacement and energy. The results are presented in tables 2
²⁰⁴ and 3, respectively.

Table 2: Displacement at failure for different loading angles

	Pure opening $\psi = 0°$	Mixed opening/shear			Pure shear $\psi = 90°$
		$\psi = 30°$	$\psi = 45°$	$\psi = 60°$	
Test 1 (mm)	1.65	1.74	1.50	1.41	1.37
Test 2 (mm)	1.51	1.63	1.45	1.51	1.44
Test 3 (mm)	2.05	1.62	1.65	1.54	1.58
$\bar{U}_{Failure}$ (mm)	1.74	1.66	1.53	1.49	1.46
$\bar{D}$ (%)	17.5	2.94	5.14	3.42	5.31

16

Table 3: Dissipated energy for different loading angles

	Pure opening $\psi = 0°$	Mixed opening/shear			Pure shear $\psi = 90°$
		$\psi = 30°$	$\psi = 45°$	$\psi = 60°$	
Test 1(kN.mm)	13.08	16.58	13.56	19.48	22.19
Test 2(kN.mm)	11.90	15.20	15.98	18.85	23.13
Test 3(kN.mm)	18.80	15.02	18.45	20.52	25.38
$\bar{E}_{Disspated}$(kN.mm)	14.59	15.60	16.13	19.70	23.56
$\bar{D}(\%)$	19.22	4.20	9.50	3.06	5.12

The analysis of tables 1, 2 and 3 suggests that the relative average dispersion is fairly low for the ultimate forces ($< 7\%$ for $\psi = 45$ °). It is similar for the displacement at failure ($< 6\%$ for all cases except for $\psi = 0°$). Therefore, a good reproducibility in terms of dissipated energy is reported with a relative average dispersion $< 10\%$ that is an acceptable deviation and allows to valid the reproducibility for the test. This dispersion could be explained by the variation of the diameter size nugget and the quality of the spot weld nugget related to the welding procedure for the same Lot (Lot 1). Moreover, eccentricity defects between the center of the spot weld and the free zone center are identified for some tested specimens. Despite the weak tolerances imposed to manufacture the spot weld assembly, excentricity defects could be important for some specimen 15.
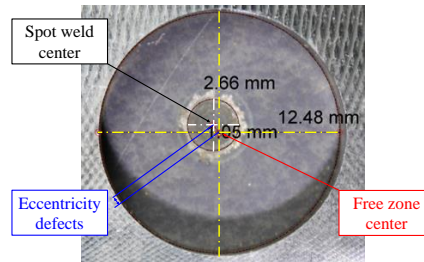

Figure 15: Illustration of an exteme eccentricity defect observed on a spot weld specimen

3.2.2. Failure modes

The post-mortem observations of the tested specimens allow to identify three principal failure modes according to the loading angle:

17

²²⁰ **Pull-out failure mode (M1):** For this mode the failure occurs around the
²²¹ spot weld nugget. This failure mode is obtained in the pure opening mode
²²² where the normal load is dominant during the test. The normal load
²²³ generates a stress concentration around the nugget that creates a crack.
²²⁴ The crack occurs due to necking/shearing throughout the thickness of the
²²⁵ Base Material (BM) near the Heat-Affected Zone (HAZ) and propagates
²²⁶ around the outline of the nugget. Thus, the weld nugget is pulling out
²²⁷ from the P3 layer (22MnB5, thickness 1.6 mm). Figure 16 shows the
²²⁸ section cut view of failed spot welds (post-mortem specimen) for the pure
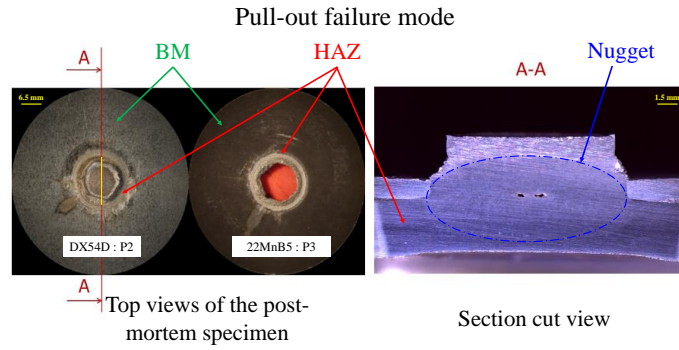²²⁹ opening mode ($\psi = 0°$).

Figure 16: Pull-out failure mode of three-sheet spot weld for opening mode ($\psi = 0°$)

²³⁰ **Inter-facial failure mode (M2):** This failure mode occurs when the shear
²³¹ load is dominant during test. The shear load generates a stress
²³² concentration at the sheet/sheet interface in the nugget level and leads to
²³³ create an inter-facial crack that propagates through the spot weld nugget
²³⁴ as shown in figure 17 that presents a section cut view of failed spot welds
²³⁵ (post-mortem specimen) for the pure shear mode ($\psi = 90°$). Thus, the
²³⁶ inter-facial mode occurs at the interface between the DX54D sheet metal
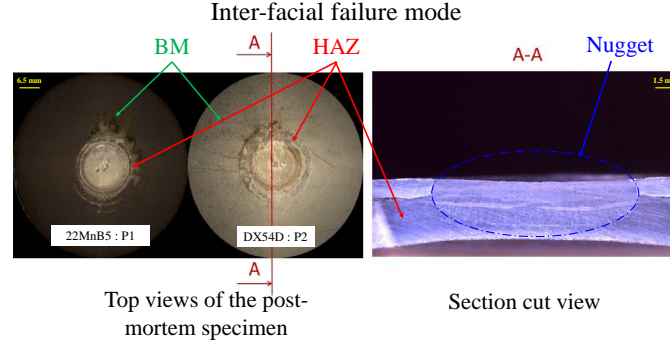²³⁷ (P2) and the thinnest thickness of the 22MnB5 sheets metal (P3).

Figure 17: Inter-facial failure mode of three-sheet spot weld for shear mode ($\psi = 90°$)

Mixed Pull-out/Inter-Facial failure mode (M3): It is a combination of the two previous presented failure modes as Pull-out/Inter-facial mode. This mode of failure occurs in the mixed opening/shear mode where the normal and shear loads are combined during test. The combined loads generate a stress concentration at the spot weld nugget that causes the deformation of the nugget at its mid thickness following the loading direction. Therefore, the principal axis of the nugget remains almost collinear with the loading direction. Thus, the normal load increases and becomes more dominant than the shear load. The opening mode conditions came back and lead to the pull out of the deformed weld nugget from the thinnest thickness of the 22MnB5 sheets metal (P3). After this last phase, the deformed nugget can interact with the central sheet leading to the progressive opening observed in figure 19. In fact, the post peak force is due to the plastic bending of the central sheet.

Figure 18 illustrates the observed mixed failure mode through a section cut view of failed spot weld (post-mortem specimen) for the mixed opening/shear mode $\psi = 60°$).
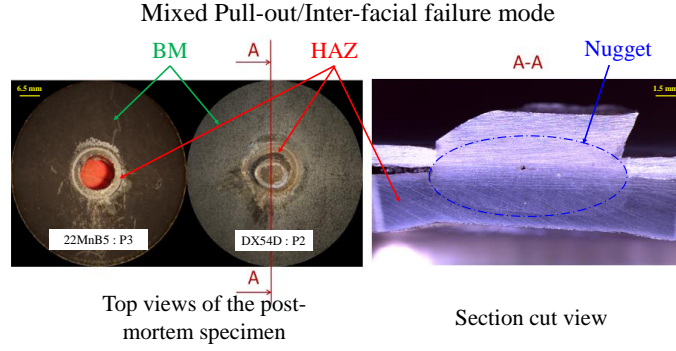
Mixed Pull-out/Inter-facial failure mode

Figure 18: Mixed Pull-out/Inter-facial failure mode of three-sheet spot weld for mixed opening/shear mode ($\psi = 60°$)
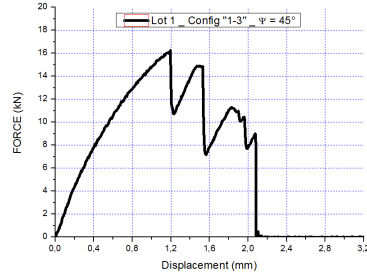

Figure 19: Typical force vs. displacement response of three-sheet spot weld assembly

Table 4 presents the different failure modes observed for different loading angles.

Table 4: Failure modes for different loading angles

	Pure opening $\psi = 0°$	Mixed opening/shear $\psi = 30°$	$\psi = 45°$	$\psi = 60°$	Pure shear $\psi = 90°$
Failure Mode	M1	M1	M3	M3	M2

As a conclusion, three principal failure modes as Pull-out, Inter-facial and

Mixed Pull-out/Inter-facial are identified during experiments. The occurrence of such a mode is related to the loading conditions (pure opening, pure shear and mixed opening/shear). For a better understanding for these failure modes, Vickers hardness mapping test was performed on a specimen cut perfectly in the spot weld nugget center. A Future Tech Hardness Tester (Model FM) was used with a loading force of 300 g. The hardness distribution results allows to identify three characteristic zones of spot weld: Nugget, Heat Affected Zone (HAZ) and Base Material (BM) (Figure 20). A mapping step of 1 mm is used for the base material and 0.1 mm is used for the HAZ and the nugget.
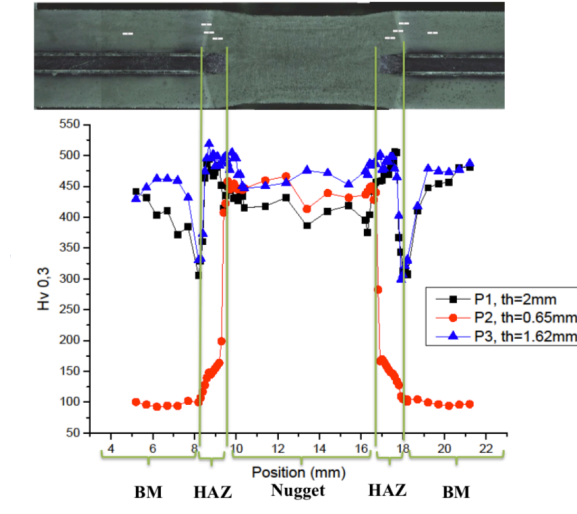

Figure 20: Hardness distribution along the spot weld joint assembly

4. Discussion of the experimental results

The analysis of the mechanical behaviour and the failure modes of the studied three-sheet spot welded assembly in the different loading conditions allows to investigate the influence of the loading angle and the effect of the nugget quality (nugget diameter size) on the ultimate force, the displacement at failure and the dissipated energy.

21

²⁷³ *4.1. Effect of the loading angle*

²⁷⁴ Based on the obtained results (Tabs. 1 and 2), the mean ultimate force
²⁷⁵ ($\bar{F}_{Ultimate}$) vs. the loading angle (ψ) is presented in figure 21. The mean
²⁷⁶ ultimate force increases exponentially. Indeed, between $\psi = 0°$ and $\psi = 30°$ the
²⁷⁷ force is almost constant. Beyond of $\psi = 45°$, a significant increase of the force is
²⁷⁸ reported to reach the maximum of $\bar{F}_{Ulimate} = 27.71kN$ for $\psi = 90°$. However,
²⁷⁹ considering the mean displacement at the failure, figure 21 (b) shows that it
²⁸⁰ decreases when the loading angle increases contrary to the ultimate force. The
²⁸¹ minimum mean displacement at failure $\bar{U}_{Ultimate}= 1.46mm$ is reached for the
²⁸² loading angle $\psi = 90°$.

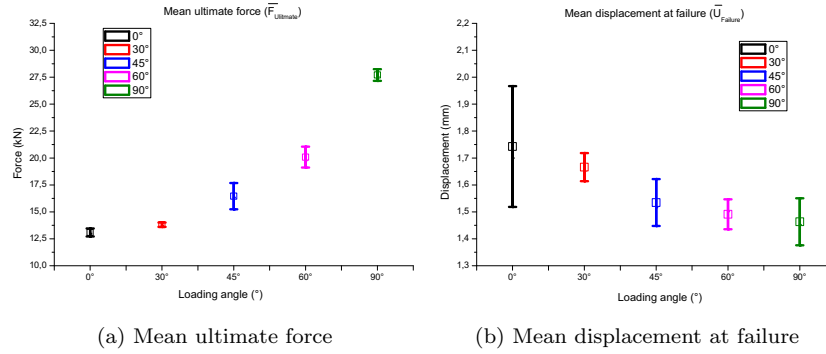(a) Mean ultimate force   (b) Mean displacement at failure

Figure 21: Effect of the loading angle ψ (a) Mean ultimate force and (b) Mean displacement
at failure

²⁸³ The mean dissipated energy vs. the loading angle is presented in figure
²⁸⁴ 22.a The mean dissipated energy increases with the loading angle. Indeed, the
²⁸⁵ failure for the pure shear mode requires an important quantity of energy when
²⁸⁶ compared to the failure mode for the pure opening mode. Thus, a comparison
²⁸⁷ between the two failure modes is presented in figure 22.b in order to explain the
²⁸⁸ trend of dissipated energy evolution with the loading angle.
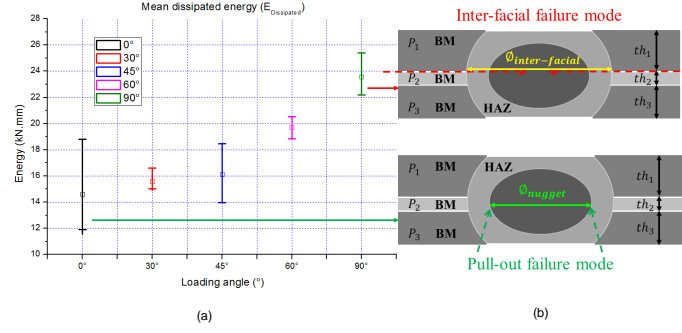
22

Figure 22: (a) Effect of the loading angle on the mean dissipated energy. (b) Illustrative scheme of the two failure modes

For the Pull-out failure mode, the rupture occurs around the spot weld nugget in the HAZ (where hardness has been measured at 300 Hv Figure; 20) with a Pull-out failure section equal to 14.45 mm^2, which can be calculated using Eq. 5.

$$S_{Pull-out} = \pi \times \phi_{nugget} \times th_3 \tag{5}$$

where $\phi_{Pull-out}$ is the nugget spot weld diameter and th_3 the P3 thickness (fig. 22).

However, for the Inter-facial failure mode, the rupture occurs at the interface P2/P1 across the nugget spot weld (where hardness has been measured at 460 Hv) with a Inter-facial failure section equal to 50 mm^2, calculated using Eq. 6:

$$S_{Inter-facial} = \pi \times \phi^2_{Inter-facial}/4 \tag{6}$$

where $\phi_{Inter-facial}$ is the spot weld diameter (fig. 22).

The great difference in the failure cross-sections and material properties in the crack path explain the increase in dissipated energy when the loading angle increase.

23

4.2. Effect of the nugget spot weld diameter

Three nugget diameters are considered for the three-sheet spot welded assembly: 6.5 mm, 7.2 mm and 3.7 mm. They correspond respectively to the three lots, Lot 1, Lot 2 and Lot 3 (figure 2). Figure 23 presents the effect of the spot weld nugget diameter on the ultimate force and the dissipated energy. For a given loading angle, the ultimate force and the dissipated energy increase when the nugget spot weld diameter increases. These results present a good agreement with the published previous works [10, 11, 12, 13, 14, 15]. A significant combined effect of the loading angle and the nugget spot weld diameter is observed on the ultimate force and the dissipated energy. For instance, considering the two conform nugget spot welded specimens (Lot 1 and Lot 2), figure 23 shows no effect of the nugget spot weld diameter on the ultimate force and dissipated energy for $\psi = 0°$, a small effect for $\psi = 30°$ and a pronounced effect for $\psi = 90°$.

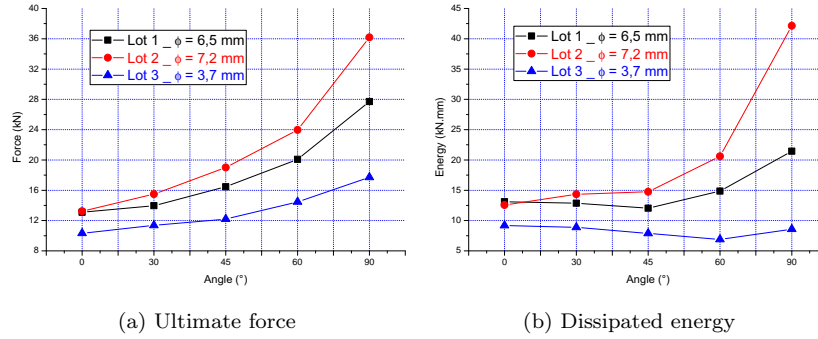(a) Ultimate force   (b) Dissipated energy

Figure 23: Effect of the nugget spot weld diameter on the (a) ultimate force and (b) dissipated energy

The effect of the nugget spot weld diameter is also highlighted in figure 24) by superimposing the three rupture envelopes expressed by normal force component $N = \cos(\psi)$ vs. shear force component $S = \sin(\psi)$ for each lot. Whatever the loading angle, the dependency of the failure force to the spot weld diameter is obvious: the bigger the nugget, the higher the failure force.

Note that a force-based criterion of the form Eq. 7 [4] could be identified if required for each lot based on Figure 24.
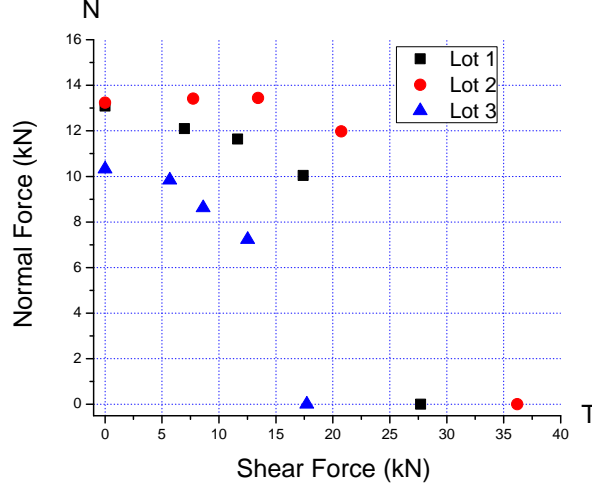

Figure 24: Effect of the nugget spot weld diameter on N-T diagram

$$(\frac{N}{N_u})^a + (\frac{T}{T_u})^b = 1 \tag{7}$$

where N_u is the ultimate normal force at failure obtained for $\psi = 0°$, T_u is the ultimate tangential force at failure obtained for $\psi = 90°$, a and b are exponents of the failure criterion identified from the experimental results of the combined loading tests.

5. Analysis of the dynamic loading sensitivity of three-sheet multi-material spot welded assemblies

5.1. Strain rate effect on the base material (22MnB5)

The three sheet spot welded assembly is composed by two steel grades : 22MnB5 ultra-high strength steel (UHSS) and DX54D mild steel. The DX54D mild steel grade is classified as an alloy quality low carbon steel. The mechanical behaviour and mechanical properties of the DX54D mild steel have been deeply

25

³³⁴ investigated on a large range of plastic strain rates and extensively reported
³³⁵ in the literature. The 22MnB5 is classified as ultra-high strength steel. Its
³³⁶ mechanical properties are extremely high comparing by DX54D mild steel.
³³⁷ Table 5 presents the quasi-static mechanical properties of 22MnB5 and DX54D
³³⁸ steels in terms of engineering stress and strain (data given by our industrial
³³⁹ partner).

Table 5: 22MnB5 and DX54D base material properties

	22MnB5	DX54D
R_m - Tensile strength (MPa)	1500	260-360
R_e - 0.2% proof strength (MPa)	1100	120-220
A - Min. elongation $L_0 = 80$ mm (%)	34-36	6

³⁴⁰ The mechanical behaviour of the 22MnB5 base material is investigated under
³⁴¹ quasi-static and dynamic loadings in to order to check its strain rate sensitivity.
³⁴² In the first step, quasi-static tests are realised using a high speed hydraulic
³⁴³ machine (INSTRON VHS 65/20) with an imposed load speed $V_{QS} = 19 \times 10^{-3}$
³⁴⁴ m/s. A good correlation is observed with the mechanical properties reported in
³⁴⁵ table 5.

³⁴⁶ In the second step, dynamic tests are realised using a pre-stretched
³⁴⁷ Hopkinson bars device. The pre-stretched bar technique is used her to acces
³⁴⁸ to moderate strain rate, thus [100;1000] /s; Theses bars are made of mar-aging
³⁴⁹ steel and composed of two cylindrical bars with 11 mm in diameter and 7 m
³⁵⁰ in length. The device is accurately aligned along a rigid I-beams frame and
³⁵¹ instrumented with strain gages so as to be calibrated as forces and velocities
³⁵² sensors. Details of equations, assumptions and analysis can be found in [16].
³⁵³ Three impact velocities are applied as $V_D = 1.3$ m/s, 3.5 m/s and 5.65 m/s ($\dot{\varepsilon}$
³⁵⁴ (/s) = 125 , 350 and 550). Figure 25 presents the mean curves of the quasi-static
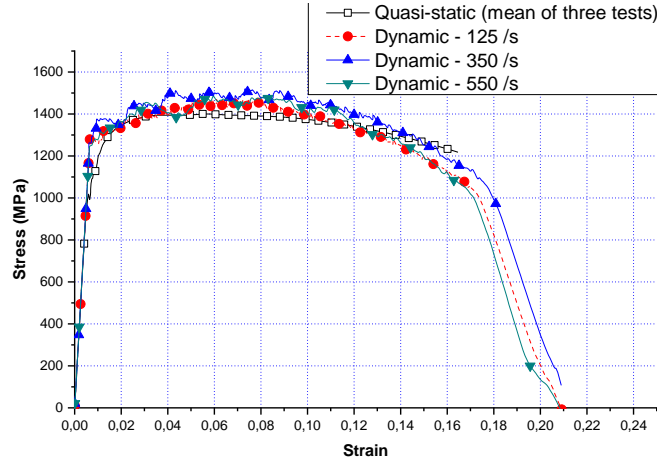³⁵⁵ stress vs. strain responses and the dynamic ones.

26

Figure 25: Strain rate effect of the base material 22MnB5 behaviour

The analysis of these curves shows two different tendencies. On the one hand, the hardening of the 22MnB5 UHSS base material is quite insensitive to the strain rate. One the other hand, the strain at failure seems to decrease with the strain rate. It can be related that the 22MnB5 UHSS base material is strain rate insensitive in the tested range.

5.2. Loading velocity sensitivity of the spot welded assembly

In a first step, it is proposed to evaluate the sensitivity of the assembly to the loading velocity in a low range by considering hydraulic jack experiment responses. A velocity jump of two decades ($V_1 = 0.001 m/s$ and $V_2 = 0.1 m/s$) and the angles $\psi = 0$, 30 and 60 ° are considered. No significant effect is observed on the ultimate force, displacement at failure, and energy (Figures 26, 27)
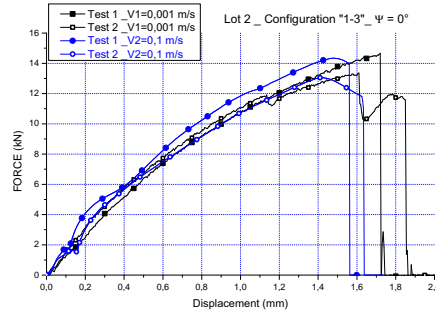
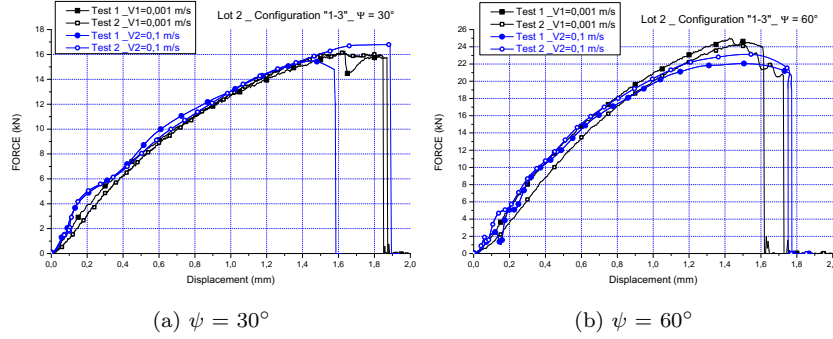Figure 26: Loading velocity sensitivity under the pure opening load mode ($\psi = 0$ °)

(a) $\psi = 30°$

(b) $\psi = 60°$

Figure 27: Loading velocity sensitivity under mixed modes (I/II) (a) $\psi = 30°$ and (b) $\psi = 60°$

In a second step it is proposed to evaluate the sensitivity of the assembly to the loading velocity in an higher range by comparing hydraulic jack experiment responses ($V_1 = 0.001 m/s$ and $V_2 = 0.1 m/s$) with Split Hopkinson Tension Bars experiment repsonses ($V_3 = 4 m/s$) for a loading angle of $\psi = 0°$.

A set of classical HSS bars used in tension thanks to a hollow projectile made of aluminium is proposed to test under dynamic condition a 3 sheets spot welds . The bars have a 30 mm diameter for a total length of 12 m. [17]
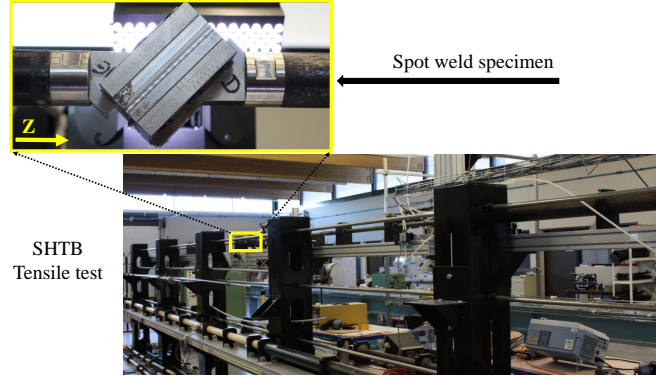
28

Figure 28: Split Hopkinson Tension Bars set-up for testing of spot-welded specimens under dynamic loading conditions

The raw signals of the SHTB tests are shown in Figure 29. The incident and transmitted waves are in accordance with what can be expected in classical data acquisition. However, the reflected wave reveals a peak which is expected to come from the section change caused by the mounting of the device along the bars. Thus this raw reflected signal cannot be considered as it is, and needs in fact to be rebuilt in accordance with the methodology presented in reference [16], i.e. considering a correct energy balance. In details, the reflected wave is rebuilt by subtraction of incident and transmitted waves. This new signal is used for the calculation of the specimen elongation. The transmitted wave which is less affected by the setup disturbances and the inertia effect is still used for the force calculation. The presented force-displacement curves related to the SHTB tests at $V_3 = 4m/s$ are following this methodology (figure 30).
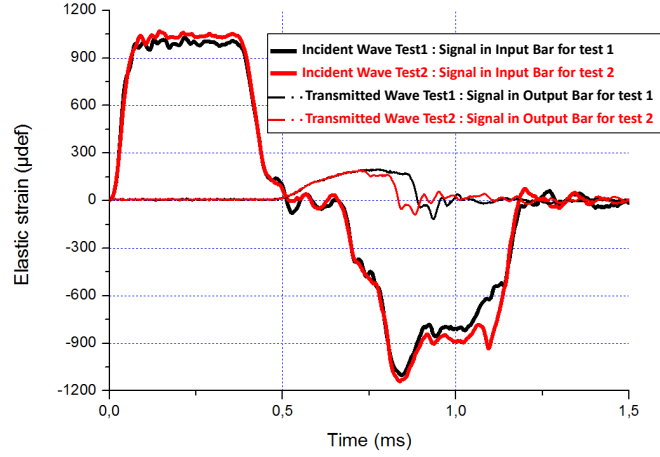
Figure 29: Raw signals from SHTB tests

Figure 30 compares the Force vs Displacement responses between quasi-static loading $(V_1 = 0.001m/s)$ and both dynamic ones $(V_2 = 0.1m/s$ and $V_3 = 4m/s)$ for pure opening mode.
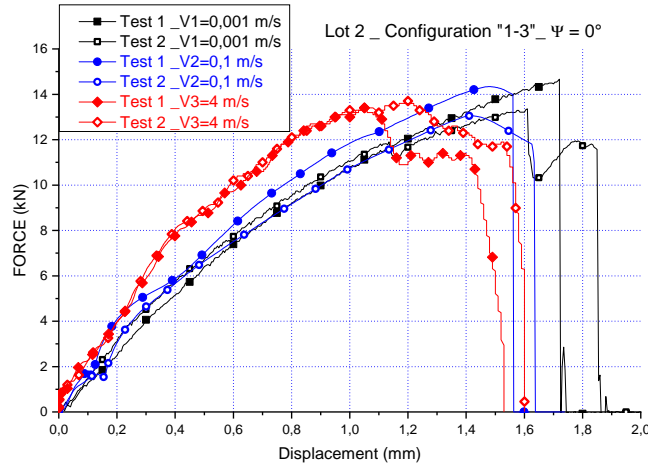

Figure 30: Loading velocity sensitivity under the pure opening load mode ($\psi = 0$ °) using SHTB system

No significant effect is reported on the ultimate force for pure opening mode.

This is in line with the rate insensitivity of the 22MnB5 constitutive material. An increase in the stiffness associated with a reduced displacement at failure, with iso energy by comparison with the lower loading velocities, suggests the existence of dynamic inertia effect. Other loading angles and higher velocities are however still necessary to confirm this preliminary suggestion.

Table 6 summarises ultimate forces, displacements at failure and dissipated energy for the different considered loading angles and velocities. These properties are presented in terms of mean values for each configuration and loading velocity.

Table 6: Mean values for ultimate forces, displacement at failure and dissipated energy for different loading angles and velocities

	Pure opening $\psi = 0°$	Mixed opening/shear	
		$\psi = 30°$	$\psi = 60°$
Ultimate force $V = 0.001m/s$ (kN)	13.95	16.08	24.54
Ultimate force $V = 0.1m/s$ (kN)	13.66	16.12	22.50
Ultimate force $V = 4m/s$ (kN)	13.55	–	–
Disp at failure $V = 0.001m/s$ (mm)	1.78	1.86	1.66
Disp at failure $V = 0.1m/s$ (mm)	1,60	1.75	1.76
Disp at failure $V = 4m/s$ (mm)	1.56	–	–
Dissipated energy $V = 0.001m/s$ (kN.mm)	15.92	19.70	26.50
Dissipated energy $V = 0.1m/s$ (kN.mm)	14.34	19.01	28.35
Dissipated energy $V = 4m/s$ (kN.mm)	14.70	–	–

6. Conclusion

The paper deals with the mechanical behaviour of multi-material multi-sheet spot welded assemblies and the failure modes under pure opening, pure shear, and mixed opening/shear modes. A three-sheet spot welded assembly combining two different steel grades (22MnB5 and DX54D) is considered with three weld nuggets diameters. The ultimate force, the displacement at failure and the dissipated energy are reported. A significant effect of the loading angle

31

is reported. This effect of the loading angle on the mechanical behaviour of the spot welded assembly is explained through a comparison of the failure modes. Three failure modes are identified : a pull-out failure mode (pure opening), an inter-facial failure mode (pure Shear) and a mixed pull-out/inter-facial mode (mixed opening/shear).

For each loading angle, three type of specimens with different spot weld nugget size are tested. The analysis of force vs. displacement responses shows that the nugget diameter has a significant effect on the ultimate force and the dissipated energy. A significant combined effect of the loading angle and the nugget spot weld diameter is observed on the mechanical response. Finally, a preliminary study of the loading velocity sensitivity of the three-sheet spot welded assembly is realized. No significant effect is reported on the ultimate force for pure opening mode. However an increase in the stiffness associated with a reduced displacement at failure suggests the existence of dynamic inertia effect which has to be confirmed by a further intensive experimental campaign with other loading angles and higher velocities. **Even if re design of the set-up could minimise the dynamic inertia effect, it would be difficult to cancel it completely. Moreover, considering the output bar signal for the force calculation appears to give satisfying results, compared to tests carried out at lower velocities on a hydraulic jack with a load cell.**

References

[1] E. Hartmann, Mechanical tests of spot welds, Welding Journal 37,(1958), 520-523.

[2] D. J. VandenBossche, Ultimate Strength and Failure Mode of Spot welds in High Strength Steels, SAE Technical Paper 770214, (1997).

[3] E. Markiewicz, P. Drazetic, Experimental and local/global numerical characterization of mechanical strength for spot-welded assemblies, Mécanique et Industries 4 (1), (2003), 17–27.

[4] Y.Lee, T. Wehner, M. Lu, T. Morrissett, E. Pakalnins, Ultimate trength of resistance spot welds subjected to combined tension, Journal of Testing and Evaluation 26 (3), (1998), 213–219.

[5] S. H. Lin, J. Pan, S.R. Wu, J. Tyan, P. Wung, Failure loads of spot welds under combined opening and shear static loading conditions, International Journal of Solids and Structures 39 (1), (2001), 19–39.

[6] S. H. Lin, J. Pan, J. Tyan, F. Prasad, A general failure criterion for spot-welds under combined loading conditions, International Journal of Solids and Structures 40 (21), (2004), 5539–5564.

[7] B. Langrand, A. Combescure, Non-linear and failure behaviour of spotwelds: a global finite element and experiments in pure and mixed modes I/II, International Journal of Solids and Structures 41 (24-25),(2004), 6631–6646.

[8] B. Langrand, E. Markiewicz, Strain-rate dependence in spot welds: Non-linear behaviour and failure in pure and combined modes I/II, International Journal of Impact Engineering 37 (7), (2010), 792–805.

[9] J. H. Song, H. Huh, Failure characterization of spot welds under combined axial–shear loading conditions, International Journal of Mechanical Sciences 53 (7),(2011), 513 – 525.

33

[10] M. S. Pouranvari, M., Failure behavior of three-steel sheets resistance spot welds : Effect of joint design, Journal of Materials Engineering and Performance 21 (8), (2012), 1669–1675.

[11] M. S. Pouranvari, M., Weld nugget formation and mechanical properties of three-sheet resistance spot welded low carbon steel, The Canadian Journal of Metallurgy and Materials Science 51 (1), (2012), 105–110.

[12] A. Tavassolizadeh, P. Marashi, M. Pouranvari, Mechanical performance of three thickness resistance spot welded low carbon steel, Materials Science and Technology 27 (1), (2011), 219–224.

[13] C. Nielsen, K. Friis, W. Zhang, N. Bay, Three-sheet spot welding of advanced high-strength steels, Welding Research, 90, (2011), 32–40.

[14] S. Wei, R. Liu, D. Lv, L. Lin, R. Xu, Y. Guo, Weldability and mechanical properties of similar and dissimilar resistance spot welds of three-layer advanced high strength steels, Science and Technology of Welding and Joining 20 (1), (2015), 20–26.

[15] Y. Zhang, Y. Li, Z. Luo, Y. Feng, J. Zhou, Effect of joint design on the failure behaviour of three-stack-up austenitic stainless steel resistance spot welds, Science and Technology of Welding and Joining 21 (3), (2016), 484–492.

[16] G. Haugou, N. Leconte, H. Morvan, Design of a pre-stretched tension Hopkinson bar device: Configuration, tail corrections, and numerical validation, International Journal of Impact Engineering 97, (2016), 89–101.

[17] G. Haugou,B. Bourel, F. Lauro, B. Bennani, D. Lesueur, D. Morin, Characterization and modelling of structural bonding at high strain rate, 10th International Conference on the Mechanical and Physical Behaviour of Materials under Dynamic Loading, DYMAT, Freibourg, Germany,september 2012, 7598-0757-4